Open Research Online

The Open University's repository of research publications
and other research outputs

Intermediate energy cross sections for electron-impact vibrational-excitation of pyrimidine

Journal Item

How to cite:

Jones, D. B.; Ellis-Gibbings, L.; García, G.; Nixon, K. L.; Lopes, M. C. A. and Brunger, M. J. (2015). Intermediate energy cross sections for electron-impact vibrational-excitation of pyrimidine. The Journal of Chemical Physics, 143(9), article no. 094304.

For guidance on citations see FAQs.

© 2015 AIP Publishing LLC.

https://creativecommons.org/licenses/by-nc-nd/4.0/

Version: Accepted Manuscript

Link(s) to article on publisher's website:
http://dx.doi.org/doi:10.1063/1.4929907

Copyright and Moral Rights for the articles on this site are retained by the individual authors and/or other copyright owners. For more information on Open Research Online's data policy on reuse of materials please consult the policies page.

oro.open.ac.uk

Intermediate energy cross sections for electron-impact vibrational-excitation of pyrimidine

D. B. Jones,[1] L. Ellis-Gibbings,[2] G. García,[2] K. L. Nixon,[3,4] M. C. A. Lopes,[3] and M. J. Brunger[1,5,a)]

[1)]*School of Chemical and Physical Sciences, Flinders University, GPO Box 2100, Adelaide, SA 5001, Australia*

[2)]*Instituto de Física Fundamental, CSIC, Serrano 113-bis, 28006 Madrid, Spain*

[3)]*Departamento de Física, Universidade Federal de Juiz de Fora, 36036-330, Juiz de Fora, Minas Gerais, Brazil*

[4)]*School of Biology, Chemistry and Forensic Science, University of Wolverhampton, Wolverhampton WV1 1LY, UK*

[5)]*Institute of Mathematical Sciences, University of Malaya, 50603 Kuala Lumpur, Malaysia*

(Dated: 24 July 2015)

We report differential cross sections (DCSs) and integral cross sections (ICSs) for electron-impact vibrational-excitation of pyrimidine, at incident electron energies in the range 15–50 eV. The scattered electron angular range for the DCS measurements was 10°–90°. The measurements at the DCS-level are the first to be reported for vibrational-excitation in pyrimidine via electron impact, while for the ICS we extend the results from the only previous condensed-phase study [J. Chem. Phys. **122**, 094701 (2005)], for electron energies $\leqslant$ 12 eV, to higher energies. Interestingly, the trend in the magnitude of the lower energy condensed-phase ICSs is much smaller when compared to the corresponding gas phase results. As there is no evidence for the existence of any shape-resonances, in the available pyrimidine total cross sections [Phys. Rev. A **88**, 032702 (2013) and Phys. Rev. A **88**, 042702 (2013)], between 10–20 eV, this mismatch in absolute magnitude between the condensed-phase and gas-phase ICSs might be indicative for collective-behaviour effects in the condensed-phase results.

PACS numbers: 34.80.Gs

Keywords: electron impact, cross sections, vibrational excitation, pyrimidine

[a)]Electronic mail: (Author to whom correspondence should be addressed) Michael.Brunger@flinders.edu.au

I. INTRODUCTION

There has been significant recent interest from the electron scattering community, in respect to experimental and theoretical studies with pyrimidine. Much of this interest can be traced to pyrimidine ($C_4H_4N_2$) being a prototypical structure for the RNA/DNA bases thymine, cytosine and uracil,[1] and thus its relevance to the development of Monte Carlo simulations[2–5] that attempt to describe charged-particle interactions within living tissue. In particular we note results at the total cross section level,[6–8] elastic scattering cross sections,[9–12] some condensed-phase vibrational-excitation integral cross sections (ICSs),[13] electronic-state spectra, differential cross sections (DCSs) and ICSs,[11,13–17] ionization[18–21] and an unpublished dissociative electron attachment cross section from Field.[1,22] We note that on the basis of these data, García and colleagues recently assembled a recommended cross section data base for electron-pyrimidine scattering.[1]

When Mašín *et al.*[11] compared their gas-phase pyrimidine electronic-state ICSs to the corresponding condensed-phase results from Levesque *et al.*,[13] they found that while the sums over the electronic-state ICSs from both systems were in pretty good quantitative accord (see their Fig. 4[11]), the individual electronic-band ICSs were, in some cases, quite different. We were therefore interested to see here if such a trend was also prevalent in the pyrimidine vibrational-excitation cross sections. In addition, in our recent study of vibrational excitation in gas-phase tetrahydrofuran (THF)[23,24] we found that the magnitude of the ICSs of the various quanta remained relatively large out to at least ~50 eV and that the effect of this was to significantly affect the transport properties of electrons travelling through THF under an applied electric field.[24] This is no moot point, as if a similar behaviour were found to exist in pyrimidine then it could impact upon the charged-particle track simulation results in Fuss *et al.*[1] who truncated the vibrational ICS they employed to be effectively zero at 20 eV. This observation provides another rationale for the present investigation.

At Flinders University we have recently been interested in studying biomolecules such as THF,[23–25] α-tetrahydrofurfuryl alcohol[26–28] and pyrimidine,[11,15,16] and other molecules such as phenol[29–32] which is an important byproduct when atmospheric-pressure plasmas treat biomass. All these species are polar polyatomics with appreciable permanent dipole moments (μ) and dipole polarisabilities ($\overline{\alpha}$). Specifically, for THF we have $\mu \sim 1.63$ D[33] and $\overline{\alpha} \sim 47.08$ a.u.,[34] for α-tetrahydrofurfuryl alcohol we have $\mu \sim 2$ D[26,35] and $\overline{\alpha} \sim 70.18$ a.u.,[26,36] for pyrimidine we have $\mu \sim 2.28 - 2.39$ D[37–39] and $\overline{\alpha} \sim 59.3$ a.u.[40,41] and finally for phenol we find $\mu \sim 1.33$ D[42] and $\overline{\alpha} \sim 71.13$ a.u.[43] In our previous investigations of vibrational excitation of

THF,[23,24] α-tetrahydrofurfuryl alcohol[27] and phenol,[31,32] we found that for many of the quanta studied the angular distributions of the DCSs at 15 eV were largely quasi-isotropic with the expected forward peaking of the cross section at smaller scattered electron angles,[10,44–47] due to the molecular dipole properties, only becoming apparent at incident electron energies of ~30 eV and above. While no explanation, in the absence of any theoretical input, has yet been advanced to explain this observation, we are very interested to see if it also occurs in pyrimidine.

The structure of the rest of this paper is as follows. Details of our experimental methods and analysis procedures are given in Sec. II, with the current results and a discussion of those results being provided in Sec. III. Finally, in Sec. IV, some conclusions from this investigation will be given.

II. EXPERIMENTAL DETAILS AND ANALYSIS PROCEDURES

Typical examples of the electron energy loss spectra (EELS), measured in this study, are given in Fig. 1. Those spectra were obtained using an apparatus based at Flinders University, with an extensive description of its functionality being found in Brunger and Teubner.[48] Briefly, however, a well-collimated and mono-energetic electron beam is crossed with an orthogonal beam of pyrimidine. Typical electron fluxes were in the range 2–5 nA, as measured by a Faraday cup located after the collision. In this investigation the pyrimidine sample (Sigma-Aldrich/Austin Chemical Company, >98.9% assay) underwent repeated freeze-pump-thaw cycles to remove any dissolved gases. The pyrimidine effused out of a 0.7 mm inner diameter molybdenum capillary with the flow rate being controlled by a variable leak valve. In this study the chamber pressure during the experiments was typically in the order of $\sim 5 \times 10^{-6}$ Torr, to ensure that there were no multiple scattering effects.

The intersection of the electron and pyrimidine beams defines a collision volume, and those electrons that collided with the pyrimidine and scatter at some angle θ, known as the electron scattering angle, are energy analysed using a hemispherical deflector before being detected with a channel electron multiplier. Note that the angular range of the current EELS is 10°–90°. Further note that the overall instrumental energy resolution employed in this study was ~60 meV (full-width-at-half-maximum: FWHM), which was insufficient to resolve many of the vibrational modes from one another (see Table I). As a consequence, composite vibrational mode cross sections are reported here (see Fig. 1). Electron energy loss spectra were accumulated at each scatter-

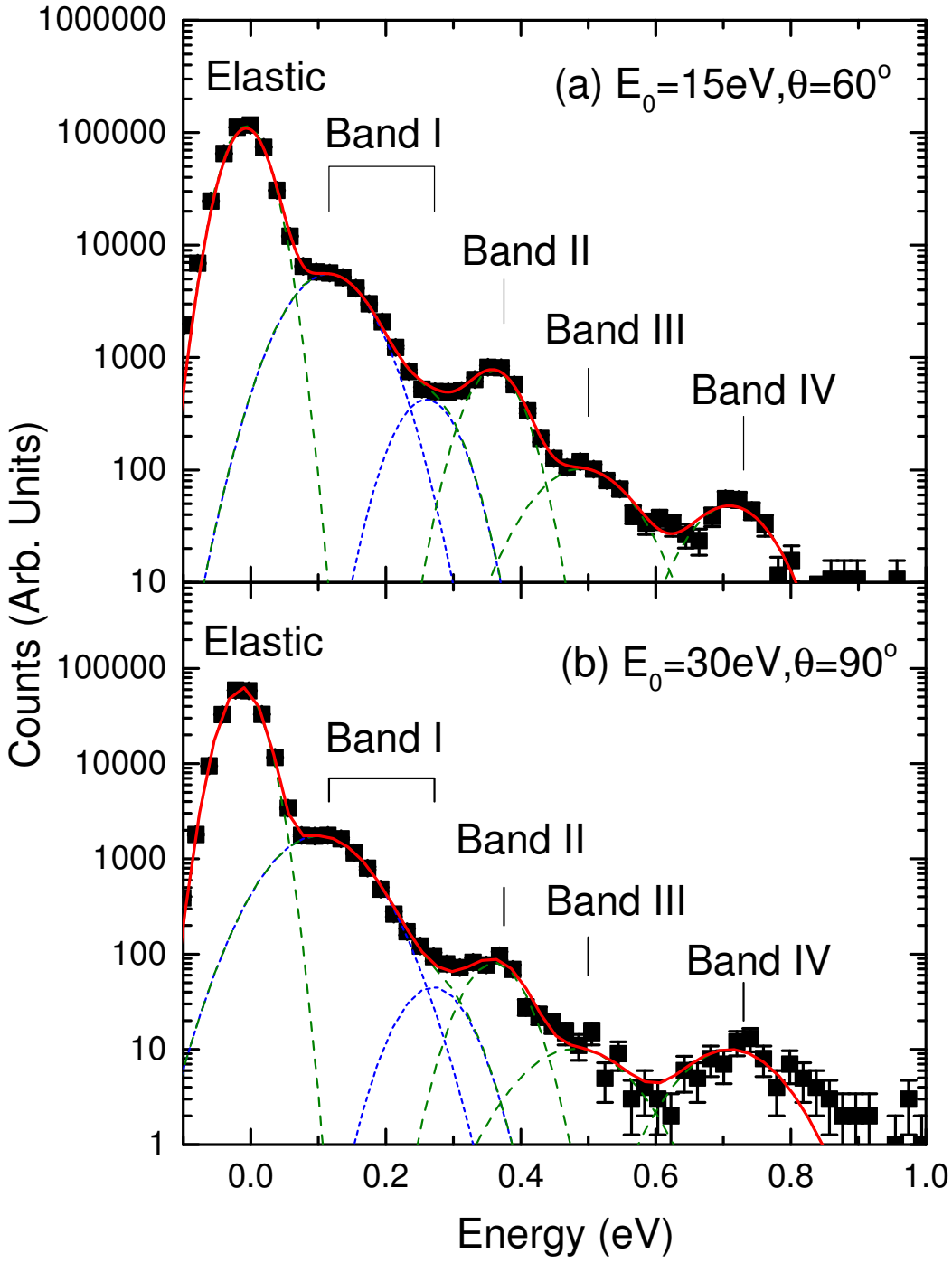

FIG. 1. Typical electron energy loss spectra of pyrimidine at (a) E_0 = 15 eV, θ = 60° and (b) E_0 = 30 eV, θ = 90° over the range −0.2 to 1.0 eV. The overall spectral deconvolution fit is denoted by the solid red line, while the fits to the various composite vibrational features are also shown by the dashed green or blue lines. The features are identified according to their Band numbers (see also Table I).

ing angle and incident energy (E_0 = 15, 20, 30, and 50 eV) by recording the number of scattered electrons detected at each energy loss value. The true electron count rate at each given energy loss was recorded using a multichannel scaler (MCS) synchronised to a linear voltage ramp that varied the detected energy loss between −0.2 eV and 1.0 eV. In this way the EELS are built up by continually scanning over the range of energy loss values, so that the possible effect of any minor variations in target beam flux or incident electron current on an EELS is minimised. Electron energy loss spectra at each E_0 and θ were repeatedly measured (2–4 times) to ensure reproducibility of the inelastic to elastic peak ratios (see later), to within the experimental uncertainty.

TABLE I. Summary of the features we assign to our electron energy loss spectra. This includes the elastic peak and the four additional vibrational composite bands we observe. Also shown are the energy loss values for each observed peak maximum, and the width of each Gaussian employed in our spectral deconvolution. Note that the vibrational excitation assignments follow Levesque *et al.*[13]

Gaussian Number	Peak Position (eV)[b]	Peak Width (eV)	Composite vibrational mode Band number	Assignments
1	0.0	0.05	–	'Elastic Peak[a]'
2	0.12	0.14	1	$\nu_{6b}, \nu_{6a}, \nu_4, \nu_{11}, \nu_1, \nu_{17a}, \nu_5, \nu_{10b}, \nu_{19a}, \nu_{19b}, \nu_{12}, \nu_{15}, \nu_{14}, \nu_3, \nu_{18b}, \nu_{9a}, \nu_{8a}, \nu_{8b}$ modes
3	0.27	0.10		
4	0.38	0.09	2	$\nu_{\text{CH-stretch modes}}$ ($\nu_{7b}, \nu_{13}, \nu_{20a}, \nu_2$ [13])
5	0.50	0.16	3	Various Combination Modes [13]
6	0.73	0.15	4	$2 \times \nu_{\text{CH-stretch modes}}$

[a]includes two unresolved out-of-plane ring deformations (ν_{16a}, ν_{16b}).[13]
[b]uncertainty in peak position is ±0.02 eV.

Our assignment of the various vibrational modes to the features we observe in our EELS (see Fig. 1) follows that of Levesque *et al.*,[13] with a summary of those spectral assignments being given in Table I. The respective EELS are now deconvoluted[49] into contributions arising from each individual or unresolved combination of excited vibrational states. In each case one Gaussian function was employed to describe the spectral profile of each resolvable inelastic feature and the elastic scattering peak, with typical examples of the results from those fits (in which the peak energies and peak widths are fixed in each case - see Table I) being given in Fig. 1. The amplitudes of the Gaussian functions were then varied in a least-squares fitting procedure[49] to provide the optimum fit to the meausured spectra. The ratio (R) of the area under the fitting function for each i^{th} vibrational feature to that under the elastic peak, at each E_0 and θ, is simply related to the ratio

of the differential cross sections (σ) from:

$$R_i(E_0, \theta) = \frac{\sigma_i(E_0, \theta)}{\sigma_0(E_0, \theta)}. \quad (1)$$

Note that Eq. (1) is only valid if the transmission efficiency of the analyzer remains constant over the energy loss and angular range studied, or is at least well characterised. Following a procedure similar to that of Allan,[50] an additional focusing lens (synchronised to the aforementioned linear voltage ramp) was also employed to minimise variations in the analyser transmission efficiency for electrons detected with different energy loss. Of course in this investigation the scattered electron energies are all very similar to that for the E_0 in question, so that a significant transmission effect would not be anticipated. Nonetheless, we place a conservative uncertainty of 20% on our response efficiency being unity. It follows from Eq. (1) that the product $R_i \times \sigma_0$ then gives the required composite vibrational mode DCS provided the elastic DCS (σ_0) is known. Those results, for the modes in question, can be found in Tables II–V. In the present study we have set the absolute inelastic scale by using the measured elastic DCSs from Palihawadana *et al.*[10] Note that the absolute scale and angular distributions of the measured elastic DCSs[10] were found to be in very good agreement with theoretical calculations from both Schwinger Multichannel[10] and R-matrix[11] computations. They are also in good accord with the independent experimental data from Baek *et al.*[12]

TABLE II. Differential Cross Sections ($\times 10^{-19}$ cm^2/sr) for electron impact excitation of vibrational Band I ($E_L \sim 0.12 - 0.27$ eV) for pyrimidine. The integral cross sections (ICS, $\times 10^{-19}$ cm^2) are also contained at the foot of the table. See text for further details. Errors are expressed in absolute units.

Angle	E_0=15 eV		E_0=20 eV		E_0=30 eV		E_0=50 eV	
(deg.)	σ	Err	σ	Err	σ	Err	σ	Err
15					59.3	49.1		
20	144.8	85	96.3	51.1	55.3	42.4	25.4	18.5
30	182.5	106.1	97.1	71.1	76.1	53.2	27.9	19.8
40	193.9	113.2	125	32.2	44.6	31.9	18.6	11.2
50	137.6	81.5	60.3	13	29.5	21.8	13.2	9.6
60	83.3	48.9	44.5	16.4	24.6	17.9	11.6	8.4
70	94.4	56.5	54.8	26.1	32.9	23.5	12	8.8
80	78.8	57	43.7	31.1	31.2	22.6	9.9	7.1
90	86.9	61.9	47.8	34	30.6	22.3	9.3	6.6
ICS	1638	1213	915	618	550	438	192	149

Error estimates on our inelastic composite mode vibrational DCSs are also given in Tables II–V. In this case the statistical errors associated with the scattering intensity measurements are

reasonably small ($\leqslant 2\%$). An additional error due to our analyser transmission calibration ($\sim$20%) must also be factored in, while the errors on the elastic DCSs used in our normalisation are taken directly from Palihawadana *et al.*[10] Another important source of possible uncertainty is that associated with the numerical deconvolution of the energy loss spectra, so that an allowance for this is also made in the overall inelastic DCS errors. When all these factors are combined in quadrature, the errors on our DCSs (see Tables II–V) are usually found to be in the range 22%–90%, with the largest errors only being for the first overtone of the CH-stretching modes for which the statistics were poorer due to its somewhat smaller excitation probability (see Fig. 1). Our excitation DCSs, for each of the composite modes at each incident electron energy, are also plotted in Fig. 2.

The DCS for a given scattering process, i, is related to the ICS, Q_i, through the standard formula:

$$Q_i(E_0) = 2\pi \int_0^{\pi} \sigma_i(E_0, \theta) \sin\theta d\theta. \tag{2}$$

In order to convert experimental DCS data, measured at discrete angles that span a finite angular range determined by the physical constraints of the apparatus, to an ICS, one must first interpolate/extapolate the measured data so that it covers the full angular range from 0° to 180°. Our approach to accomplish this, built around a generalised oscillator strength formalism[51] for optically allowed states (we are dealing with many infrared active modes here), has been discussed in great detail previously[11] and so we do not repeat that detail again. Rather, we simply note that the present ICSs, and the uncertainty on those data, are summarised at the foot of the respective Tables II–V and plotted in Fig. 3. Note that the errors on our ICS, as well as incorporating those from the DCS (with allowance for the $\sin\theta$ weighting factor in Eq. (2)), also include an uncertainty in determining the extrapolation of our DCS to 0° and 180°. When those factors are accounted for, the ICS errors are found to be in the range 44–80% with the precise error depending on the energy and vibrational mode in question.

III. RESULTS AND DISCUSSION

In Tables II–V and Fig. 2 we present the current differential cross section results, for electron impact excitation of the four composite vibrational bands in pyrimidine, from our experimental investigations. The incident electron energies of this work are 15, 20, 30 and 50 eV. In addition, our derived integral cross section results for each of those bands are also given at the foot of the respective Tables II–V and plotted in Fig. 3, where they are compared (where possible) to the

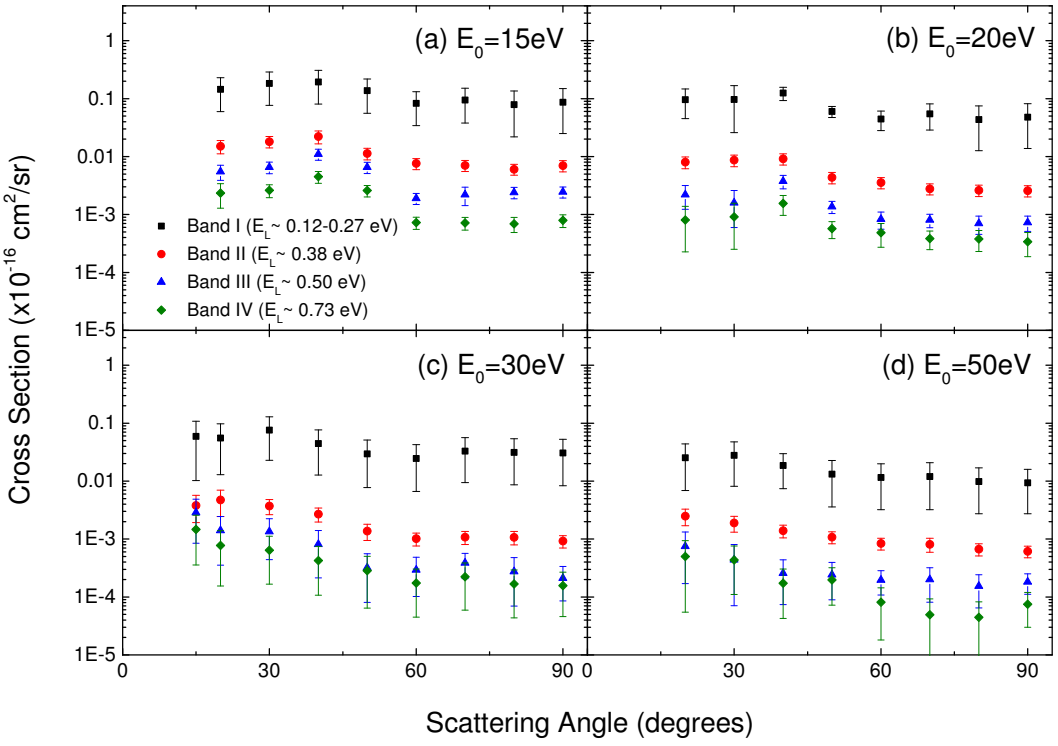

FIG. 2. Differential cross sections ($\times 10^{-16}$ cm^2/sr) for vibrational excitation of pyrimidine at various incident electron energies: (a) 15 eV, (b) 20 eV, (c) 30 eV and (d) 50 eV. Shown are the DCSs for the four vibrational bands (see also Table I) of this study: (■) Band I, (●) Band II, (▲) Band III and (◆) Band IV.

relevant condensed-phase data.[13] All the errors listed in Tables II–V and plotted in Figs. 2 and 3 are at the one standard deviation level.

Let us now consider Fig. 2 in more detail. On doing so we immediately see that, at each energy studied, the magnitude of the $\mathrm{DCSs_{Band\ I}} >> \mathrm{DCSs_{Band\ II}} > \mathrm{DCSs_{Band\ III}} > \mathrm{DCSs_{Band\ IV}}$. In addition, we find that the shape of the DCS, or angular distribution, for all four bands of composite vibrational-excitation modes is essentially quasi-isotropic at 15 eV. This behaviour, at lower energies, was also observed by us previously in our vibrational-excitation studies in THF,[23,24] α-tetrahydrofurfuryl alcohol[27] and phenol[31,32] and so is not unique to pyrimidine. What is unique to pyrimidine, compared to those other species, is that the angular distributions for the Band I vibrational modes remain quasi-isotropic at each energy (15, 20, 30, 50 eV) of this investigation. On the other hand, and consistent with the earlier THF, α-tetrahydrofurfuryl alcohol and phenol results, the vibrational angular distributions for Bands II–IV become progressively more forward peaked in magnitude (note the y-axis log-scale) as the incident electron energy is increased. This is similar to what we have observed in the past for elastic electron scattering[9–12] and electronic-state

TABLE III. Differential Cross Sections ($\times 10^{-19}$ cm^2/sr) for electron impact excitation of vibrational Band II ($E_L \sim 0.38$ eV) for pyrimidine. The integral cross sections (ICS, $\times 10^{-19}$ cm^2) are also contained at the foot of the table. See text for further details. Errors are expressed in absolute units.

Angle	E_0=15 eV		E_0=20 eV		E_0=30 eV		E_0=50 eV	
(deg.)	σ	Err	σ	Err	σ	Err	σ	Err
15					3.8	1.87		
20	15.02	3.86	8.01	1.86	4.73	2.28	2.49	0.79
30	18.16	4.08	8.67	1.96	3.73	1.09	1.89	0.58
40	22.14	5.58	9.15	2.04	2.69	0.73	1.39	0.35
50	11.33	2.54	4.37	0.98	1.38	0.43	1.08	0.25
60	7.61	1.65	3.55	0.78	1.01	0.26	0.84	0.19
70	7.05	1.53	2.78	0.6	1.08	0.27	0.81	0.22
80	6.05	1.29	2.62	0.59	1.07	0.28	0.67	0.16
90	6.99	1.54	2.57	0.56	0.92	0.22	0.61	0.14
ICS	141	65	57	25	21	10	13.7	6.5

TABLE IV. Differential Cross Sections ($\times 10^{-19}$ cm^2/sr) for electron impact excitation of vibrational Band III ($E_L \sim 0.50$ eV) for pyrimidine. The integral cross sections (ICS, $\times 10^{-19}$ cm^2) are also contained at the foot of the table. See text for further details. Errors are expressed in absolute units.

Angle	E_0=15 eV		E_0=20 eV		E_0=30 eV		E_0=50 eV	
(deg.)	σ	Err	σ	Err	σ	Err	σ	Err
15					2.85	2.01		
20	5.49	1.62	2.2	0.97	1.4	1.04	0.75	0.58
30	6.52	1.47	1.59	1	1.34	0.9	0.44	0.37
40	11.02	2.41	3.75	0.98	0.81	0.59	0.26	0.18
50	6.54	1.45	1.36	0.32	0.32	0.24	0.24	0.15
60	1.9	0.42	0.83	0.27	0.29	0.19	0.2	0.09
70	2.2	0.77	0.8	0.21	0.39	0.18	0.2	0.12
80	2.4	0.53	0.7	0.24	0.27	0.2	0.15	0.09
90	2.45	0.53	0.73	0.21	0.21	0.13	0.18	0.07
ICS	54	24	16.4	8.3	6.3	4.7	3.7	2.6

excitation in pyrimidine,[11,15,16] and in other species,[44–47] a behaviour which has been previously explained by a consideration of the target molecular dipole properties (polarisability and/or dipole moment) of the species in question. However, the degree of forward peaking in the DCS magnitude, in the elastic and discrete electronic-state excitation channels, is much more significant in those channels than what we find for the case of vibrational-excitation. While a definitive explanation for these observations awaits results from a high-level theoretical computation, we believe it must be related to the fact that for vibrational-excitation the incident electron must stimulate the nuclear degrees of freedom of the target while for elastic scattering and discrete electronic-state excitation the main interaction is between the incoming electron and the electron cloud of the tar-

TABLE V. Differential Cross Sections ($\times 10^{-19}$ cm^2/sr) for electron impact excitation of vibrational Band IV ($E_L \sim 0.73$ eV) for pyrimidine. The integral cross sections (ICS, $\times 10^{-19}$ cm^2) are also contained at the foot of the table. See text for further details. Errors are expressed in absolute units.

Angle	E_0=15 eV		E_0=20 eV		E_0=30 eV		E_0=50 eV	
(deg.)	σ	Err	σ	Err	σ	Err	σ	Err
15					1.46	1.11		
20	2.34	1.06	0.8	0.58	0.78	0.62	0.5	0.44
30	2.61	0.66	0.91	0.66	0.64	0.48	0.43	0.32
40	4.49	1.04	1.55	0.58	0.43	0.32	0.17	0.13
50	2.59	0.58	0.57	0.19	0.28	0.22	0.2	0.12
60	0.73	0.17	0.49	0.21	0.17	0.13	0.081	0.063
70	0.72	0.18	0.38	0.14	0.22	0.16	0.049	0.044
80	0.69	0.2	0.38	0.15	0.17	0.12	0.045	0.038
90	0.79	0.2	0.34	0.15	0.16	0.11	0.075	0.045
ICS	19.1	8.6	7.5	4.5	3.9	3.1	1.9	1.5

get molecule in question. In other words, while for elastic scattering and discrete electronic-state excitation the target dipole properties have a major effect on the reaction dynamics, for vibrational-excitation their role appears to be much more limited.

If we were to measure the infrared (IR) absorption spectrum of pyrimidine with a spectrophotometer,[42] then because the relevant potential surfaces are not particularly anharmonic, we would find that the intensity of the fundamental modes is significantly greater than their overtones. The results plotted in Fig. 2 for Band II, corresponding to the fundamental CH-stretch modes, and Band IV, corresponding to the overtones of those same stretch modes (see also Fig. 1), are found to be largely consistent with what one would expect on the basis of the IR-photon absorption data; namely that at each energy studied the angular distributions of the fundamental $\nu_{\mathrm{CH-stretch}}$ modes and overtone $2 \times \nu_{\mathrm{CH-stretch}}$ modes are almost identical and that, again at each E_0, the magnitudes of the DCSs for the fundamental stretch modes are significantly larger, across all measured θ, than those of the first overtone modes.

In Fig. 3 we now plot the present integral cross sections for the composite vibrational-mode Bands I, II, III and IV and the ICS for the sum of all those bands. Consistent with our earlier observation at the DCS level, here we note that the $\mathrm{ICS_{Band\ I}} >> \mathrm{ICS_{Band\ II}} > \mathrm{ICS_{Band\ III}} > \mathrm{ICS_{Band\ IV}}$. Indeed, at each E_0, the ICS for Band I contributes ~90% to the sum of the ICS for the bands in question. Additionally, we also observe that the energy dependence of the ICSs for each band are, to within the stated uncertainties, very similar. The condensed-phase vibrational excitation ICS results of Levesque *et al.*,[13] for Bands I and II, are plotted in Fig. 3 where they are compared to

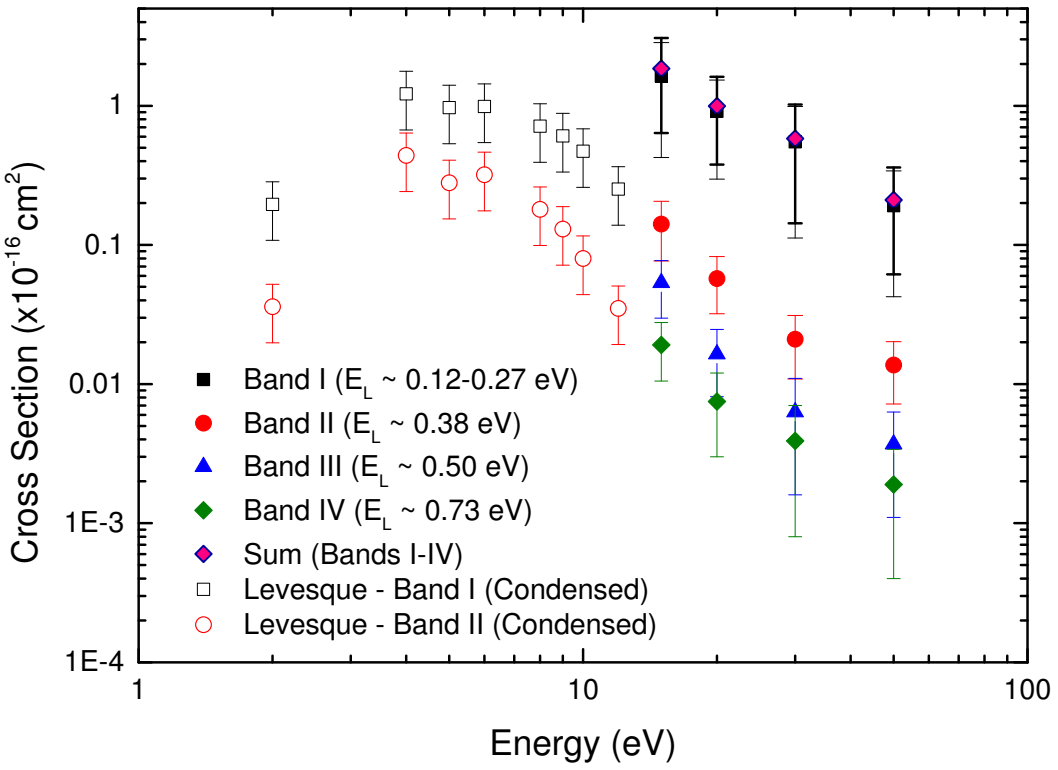

FIG. 3. Integral cross sections ($\times 10^{-16}$ cm^2) as a function of the incident electron energy for vibrational excitation of the four vibrationl bands (see also Table I) of this study: (■) Band I, (●) Band II, (▲) Band III and (◆) Band IV. Also shown is the sum of the ICSs of Bands I–IV (◆). The corresponding condensed-phase data from Levesque *et al.*[13] for Band I (□) and Band II (○) are plotted.

the corresponding present results. While the trends (i.e. energy dependencies) in the ICS for the condensed-phase and free-molecule gas phase results are largely consistent, for both sets of data, we note the significant mismatch in their absolute magnitudes. Indeed for both Bands I and II the trend in the condensed-phase ICSs is about a factor of 10 lower in value than what we find in the current study. This result has immediate ramifications for the work of Fuss *et al.*,[1] who in their charged-particle track simulation studies with pyrimidine used the cross sections from Levesque *et al.*[13] to form their vibrational-excitation data base. The present results will also be of direct relevance to any investigations seeking to model, using Monte Carlo and/or Boltzmann equation procedures,[52–54] the transport properties of electrons in a pyrimidine medium under the influence of an applied electric field. We have recently seen, for the particular species THF,[24] that the magnitude and energy extent of the ICS can play an important role in the transport behaviour of the electrons, in certain regions of E/N (E = applied electric field; N = number density), and we expect this would again be the case here.

IV. CONCLUSIONS

We have reported results from measurements of differential and integral cross sections for excitation of four composite vibrational-excitation bands in pyrimidine. The DCS results are original, there being no other experiment or theory available in the literature against which we can compare them. In terms of their angular behaviour, as we also saw previously for vibrational excitation in THF,[23,24] α-tetrahydrofurfuryl alcohol[27] and phenol,[31,32] the lowest energy (15 eV) result for each of the four bands was largely quasi-isotropic. Indeed for Band I the angular distributions were quasi-isotropic at each energy studied. However, for Bands II, III and IV the shapes of their DCSs did become more forward peaked in magnitude as you went to the higher incident electron energies. It was previously found in pyrimidine for elastic scattering[9–12] and electronic-excitation[11,15,16] that the target molecular dipole properties (polarisability and dipole moment) played a key role in their scattering dynamics, consistent with results from other scattering systems.[44–47] However for vibrational-excitation, which intrinsically involves the excitation of the nuclear degrees of freedom, it appears that the target dipole properties do not play such an important role in the collision process with *ab initio* quality scattering computations being needed to quantify the reaction mechanisms here.

In terms of the integral cross sections, for Bands I and II we can directly compare the present results with those from the condensed-phase measurements of Levesque *et al.*[13]. Here we found that while for each of the bands there was a good qualitative correspondence (i.e. in terms of the energy dependence of the ICS) between the condensed-phase and gas-phase ICS results, the gas phase results were about an order of 10 greater in magnitude. This possibly suggests some sort of collective behaviour phenomenon in the condensed phase, which has the effect of 'damping' the strength of the vibrational excitation processes relative to what we find for free-molecules in the gas phase. Certainly this is an important results in terms of the charged-particle track simulation work of Fuss *et al.*,[1] whose data base utilised vibrational ICSs in pyrimidine that were based on the work of Levesque *et al.*[13] which are apparently too small in magnitude and do not extend over a wide enough energy range.

ACKNOWLEDGMENTS

This work was supported by the Australian, Brazilian and Spanish Governmental Funding Agencies (ARC, CNPq, CAPES and MINECO). D.B.J. thanks the ARC for a Discovery Early

Career Researcher Award. R.F.C.N. acknowledges CNPq and Flinders University for financial assistance, while M.J.B. thanks CNPq for his 'Special Visiting Professor' award and the University of Malaya for his 'Icon Professor' award. M.C.A.L. acknowledges financial support from CNPq and FAPEMIG, while G.G. acknowledges financial support from MINECO (FIS2012-31230) and COST (MP1002, CM1301).

REFERENCES

[1]M. C. Fuss, L. Ellis-Gibbings, D. B. Jones, M. J. Brunger, F. Blanco, A. Muñoz, P. Limão-Vieira, and G. García, J. Appl. Phys. **117**, 214701 (2015).

[2]S. Agostinelli *et al.*, Nucl. Instrum. Methods Phys. Res., Sect. A **506**, 250 (2003).

[3]F. Salvat, J. M. Fernandez-Varea, and J. Sempau, in PENELOPE2011: A Code System for Monte-Carlo Simulation of Electron and Photon Transport, OECD–Nuclear Energy Agency (2011).

[4]C. Champion, C. Le Loirec, and B. Stosic, Int. J. Radiat. Biol. **88**, 54 (2012).

[5]A. G. Sanz, M. C. Fuss, A. Muñoz, F. Blanco, P. Limão-Vieira, M. J. Brunger, S. J. Buckman, and G. García, Int. J. Radiat. Biol. **88**, 71 (2012).

[6]W. Y. Baek, A. Arndt, M. U. Bug, H. Rabus, and M. Wang, Phys. Rev. A **88**, 032702 (2013).

[7]M. C. Fuss, A. G. Sanz, F. Blanco, J. C. Oller, P. Limão-Vieira, M. J. Brunger, and G. García, Phys. Rev. A **88**, 042702 (2013).

[8]A. Zecca, L. Chiari, G. Garcia, F. Blanco, E. Trainotti, and M. J. Brunger, J. Phys. B **43**, 215204 (2010).

[9]J. B. Maljković, A. R. Milosavljević, F. Blanco, D. Šević, G. García, and B. P. Marinković, Phys. Rev. A **79**, 052706 (2009).

[10]P. Palihawadana, J. Sullivan, M. Brunger, C. Winstead, V. McKoy, G. Garcia, F. Blanco, and S. Buckman, Phys. Rev. A **84**, 062702 (2011).

[11]Z. Mašín, J. D. Gorfinkiel, D. B. Jones, S. M. Bellm, and M. J. Brunger, J. Chem. Phys. **136**, 144310 (2012).

[12]W. Y. Baek, M. U. Bug, and H. Rabus, Phys. Rev. A **89**, 062716 (2014).

[13]P. L. Levesque, M. Michaud, and L. Sanche, J. Chem. Phys. **122**, 094701 (2005).

[14]M. H. Palmer, I. C. Walker, M. F. Guest, and A. Hopkirk, Chem. Phys. **147**, 19 (1990).

[15]D. B. Jones, S. M. Bellm, P. Limão-Vieira, and M. J. Brunger, Chem. Phys. Lett. **535**, 30 (2012).

[16]D. B. Jones, S. M. Bellm, F. Blanco, M. Fuss, G. García, P. Limão-Vieira, and M. J. Brunger, J. Chem. Phys. **137**, 074304 (2012).

[17]I. Linert and M. Zubek, Chem. Phys. Lett. **624**, 1 (2015).

[18]I. Linert, M. Dampc, B. Mielewska, and M. Zubek, Eur. Phys. J. D **66**, 20 (2012).

[19]J. D. Builth-Williams, S. M. Bellm, D. B. Jones, H. Chaluvadi, D. H. Madison, C. G. Ning, B. Lohmann, and M. J. Brunger, J. Chem. Phys. **136**, 024304 (2012).

[20]W. Wolff, H. Luna, L. Sigaud, A. C. Tavares, and E. C. Montenegro, J. Chem. Phys. **140**, 064309 (2014).

[21]C. Champion, M. A. Quinto, and P. F. Weck, Eur. Phys. J. D **69**, 127 (2015).

[22]T. Field, private communication (2008).

[23]T. P. T. Do, H. V. Duque, M. C. A. Lopes, D. A. Konovalov, R. D. White, M. J. Brunger, and D. B. Jones, J. Chem. Phys. **142**, 124306 (2015).

[24]H. V. Duque, T. P. T. Do, M. C. A. Lopes, D. A. Konovalov, R. D. White, M. J. Brunger, and D. B. Jones, J. Chem. Phys. **142**, 124307 (2015).

[25]T. P. T. Do, M. Leung, M. Fuss, G. Garcia, F. Blanco, K. Ratnavelu, and M. J. Brunger, J. Chem. Phys. **143**, 144302 (2011).

[26]H. V. Duque, L. Chiari, D. B. Jones, P. A. Thorn, Z. Pettifer, G. B. da Silva, P. Limão-Vieira, D. Duflot, M.-J. Hubin-Franskin, J. Delwiche, F. Blanco, G. García, M. C. A. Lopes, K. Ratnavelu, R. D. White, and M. J. Brunger, Chem. Phys. Lett. **608**, 161 (2014).

[27]H. V. Duque, L. Chiari, D. B. Jones, Z. Pettifer, G. B. da Silva, P. Limão-Vieira, F. Blanco, G. García, R. D. White, M. C. A. Lopes, and M. J. Brunger, J. Chem. Phys. **140**, 214306 (2014).

[28]L. Chiari, H. V. Duque, D. B. Jones, P. A. Thorn, Z. Pettifer, G. B. da Silva, P. Limão-Vieira, D. Duflot, M.-J. Hubin-Franskin, J. Delwiche, F. Blanco, G. García, M. C. A. Lopes, K. Ratnavelu, R. D. White, and M. J. Brunger, J. Chem. Phys. **141**, 024301 (2014).

[29]D. B. Jones, G. B. da Silva, R. F. C. Neves, H. V. Duque, L. Chiari, E. M. de Oliveira, M. C. A. Lopes, R. F. da Costa, M. T. do N. Varella, M. H. F. Bettega, M. A. P. Lima, and M. J. Brunger, J. Chem. Phys **141**, 074314 (2014).

[30]R. F. C. Neves, D. B. Jones, M. C. A. Lopes, K. L. Nixon, G. B. da Silva, H. V. Duque, E. M. de Oliveira, R. F. da Costa, M. T. do N. Varella, M. H. F. Bettega, M. A. P. Lima, K. Ratnavelu, G. García, and M. J. Brunger, J. Chem. Phys. **142**, 104305 (2015).

[31]R. F. C. Neves, D. B. Jones, M. C. A. Lopes, K. L. Nixon, E. M. de Oliveira, R. F. da Costa, M. T. do N. Varella, M. H. F. Bettega, M. A. P. Lima, G. B. da Silva, and M. J. Brunger, J.

Chem. Phys. **142**, 194302 (2015).

[32]R. F. C. Neves, D. B. Jones, M. C. A. Lopes, F. Blanco, G. García, K. Ratnavelu, and M. J. Brunger, J. Chem. Phys. **142**, 194305 (2015).

[33]D. Bouchiha, J. D. Gorfinkiel, L. G. Caron, and L. Sanche, J. Phys. B **40**, 1259 (2007).

[34]A. Zecca, L. Chiari, A. Sarkar, and M. J. Brunger, J. Phys. B **41**, 085201 (2008).

[35]P. Możejko, A. Domaracka, E. Ptasińska-Denga, and C. Szmytkowski, Chem. Phys. Lett. **429**, 378 (2006).

[36]C. Szmytkowski and E. Ptasińska-Denga, J. Phys. B **44**, 015203 (2011).

[37]G. L. Blackman, R. D. Brown, and F. R. Burden, J. Mol. Spectrosc. **35**, 444 (1970).

[38]P. Chen and R. A. Holroyd, J. Phys. Chem. **100**, 4491 (1996).

[39]Z. Kisiel, L. Pszczółkowski, J. C. López, J. L. Alonso, A. Maris, and W. Caminati, J. Mol Spectrosc. **195**, 332 (1999).

[40]C. Hättig, O. Christiansen, S. Coriani, and P. Jørgensen, J. Chem. Phys. **109**, 9237 (1998).

[41]B. Jansik, D. Jonsson, P. Sałek, and H. Ågren, J. Chem. Phys. **121**, 7595 (2004).

[42]http://cccbdb.nist.gov/ for dipole polarisabilities and IR spectra.

[43]G. B. da Silva, R. F. C. Neves, L. Chiari, D. B. Jones, E. Ali, D. H. Madison, C. G. Ning, K. L. Nixon, M. C. A. Lopes, and M. J. Brunger, J. Chem. Phys **141**, 124307 (2014).

[44]P. Palihawadana, J. P. Sullivan, S. J. Buckman, Z. Mašín, J. D. Gorfinkiel, F. Blanco, G. García, and M. J. Brunger, J. Chem. Phys. **139**, 014308 (2013).

[45]M. J. Brunger, L. Campbell, D. C. Cartwright, A. G. Middleton, B. Mojarrabi, and P. J. O. Teubner, J. Phys. B **33**, 783 (2000).

[46]H. Kato, H. Kawahara, M. Hoshino, H. Tanaka, M. J. Brunger, and Y.-K. Kim, J. Chem. Phys. **126**, 064307 (2007).

[47]H. Kato, M. Hoshino, H. Tanaka, P. Limão-Vieira, O. Ingólfsson, L. Campbell, and M. J. Brunger, J. Chem. Phys. **134**, 134308 (2011).

[48]M. J. Brunger and P. J. O. Teubner, Phys. Rev. A **41**, 1413 (1990).

[49]L. Campbell, M. J. Brunger, P. J. O. Teubner, B. Mojarrabi, and D. C. Cartwright, Aust. J. Phys. **50**, 525 (1997).

[50]M. Allan, J. Phys. B **38**, 3655 (2005).

[51]E. N. Lassettre, J. Chem. Phys. **43**, 4479 (1965).

[52]R. D. White, M. J. Brunger, N. A. Garland, R. E. Robson, K. F. Ness, G. García, J. de Urquijo, S. Dujko, and Z. Lj. Petrović, Eur. Phys. J. D **68**, 125 (2014).

[53]J. de Urquijo, E. Basurto, A. M. Juárez, K. F. Ness, R. E. Robson, M. J. Brunger, and R. D. White, J. Chem. Phys. **141**, 014308 (2014).

[54]K. F. Ness, R. E. Robson, M. J. Brunger, and R. D. White, J. Chem. Phys. **136**, 024318 (2012).